

Design of a compact ring for proton radiation applications

Guang-Rui Li(李光锐)^{1,2,3,1)} Shu-Xin Zheng(郑曙昕)^{1,2,3} Hong-Juan Yao(姚红娟)^{1,2,3}
 Xia-Ling Guan(关遐令)^{1,2,3} Xue-Wu Wang(王学武)^{1,2,3} Wen-Hui Huang(黄文会)^{1,2,3}

¹Key Laboratory of Particle & Radiation Imaging (Tsinghua University), Ministry of Education, Beijing 100084, China

²Laboratory for Advanced Radiation Sources and Application, Tsinghua University, Beijing 100084, China

³Department of Engineering Physics, Tsinghua University, Beijing 100084, China

Abstract: This paper presents the design of a compact proton synchrotron, including lattice structure, injection system and extraction system, for radiation applications. The lattice is based on a DBFO cell and shows good properties like small β_{\max} and decent kick arm. Radiation applications require relative strong and continuous beam, so we propose strip injection and resonance extraction for the design. A phase space painting scheme is designed and simulated by ORBIT. The scheme achieves good uniformity in phase space. The extraction system is designed and optimized by multi-particle tracking.

Keywords: proton synchrotron, lattice design, strip injection, slow extraction, RF-KO

PACS: 29.27.Ac, 29.20.dk **DOI:** 10.1088/1674-1137/41/1/017001

1 Introduction

Proton beams have many applications, like isotope production, proton therapy and single event effect (SEE) studies. For applications like proton therapy and SEE studies, it is preferred that beam energy should vary from 60 to 250 MeV. A compact proton synchrotron can fulfill this requirement well.

The difficulties of designing such a compact proton synchrotron include: (1) limited free space to accommodate RF, injection and extraction system; (2) small kick arm; (3) beam intensity limited by strong space charge effect during injection stage; and (4) controlling the ripple of the extraction beam. In this paper, we present a design which can solve these obstacles. The lattice structure is based on a DBFO cell. A strip injection section is adopted to achieve relatively high beam intensity. Beam extraction using 3rd order resonance and RF-Knockout (RF-KO) technology is designed and optimized to realize good spill quality.

2 Lattice design

The gap between circulating beam and extraction beam at a magnetic septum can be given by

$$\Delta x_{MS} = \theta \sqrt{\beta_k \beta_s} \sin \Delta \mu_{k,s} \quad (1)$$

where θ is the deflection angle at the wire septum, β_k is the value of the horizontal betatron amplitude function β_x at the wire septum, β_s is the value of the hor-

izontal betatron amplitude function β_x at the magnetic septum, and $\Delta \mu_{k,s}$ is the horizontal phase advance between the wire septum and magnetic septum. We define kick arm as $\sqrt{\beta_k \beta_s} \sin \Delta \mu_{k,s}$. Small kick arm will increase the strength required of the wire septum. A good design of lattice structure for energy level of 250 MeV should solve the problems of limited free space and kick arm. There are several available lattice designs for reference [2–7], each of which has its considerations and advantages. Some designs use just a dipole with edge angle to build the ring, which provides much free space. However, this may cause relatively small kick arm and difficulty in working point adjustment. Some designs have adopted a strong focusing structure and leave free space by putting quadrupoles close to dipoles. These designs provide good adjustment ability but may still have a disadvantage in kick arm.

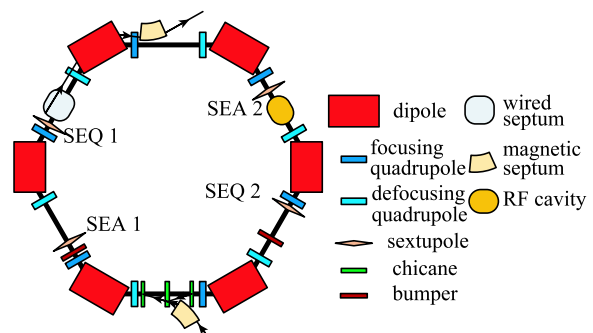


Fig. 1. (color online) Schematic layout of the ring.

Received 17 February 2016, Revised 1 August 2016

1) E-mail: ligr12@mails.tsinghua.edu.cn

©2017 Chinese Physical Society and the Institute of High Energy Physics of the Chinese Academy of Sciences and the Institute of Modern Physics of the Chinese Academy of Sciences and IOP Publishing Ltd

In our design, we use a DBFO cell as the basic component, where “D” and “F” represent defocusing and focusing quadrupole, “B” represents dipole, and “O” represents drift space. The optics of a DBFO cell are similar to those of a FODO cell, so it can easily be changed by tuning the strength of the quadrupoles to satisfy different requirements during the injection and extraction stages. DBFO cells also have the merit of leaving a long continuous free space to accommodate each accelerator system. The ring is composed of 6 identical DBFO cells. During the extraction stage, the horizontal phase advance of one cell will be tuned to about 100° , making the ring’s horizontal tune $\nu_x \approx 5/3$, so we can adopt 3rd order resonance extraction. The magnetic septum is placed near the focusing quadrupole to achieve large β_s . The wire septum is placed one cell before the magnetic septum, and the position is chosen to make $\Delta\mu_{k,s}$ close to 90° . This arrangement can also give β_k a reasonably large value. We can therefore achieve a decent kick arm, as Eq. (1) suggests.

A toy lattice based on this idea was published in a previous paper [1]. After that, we modified the structure to satisfy the requirements of magnet construction. The final layout is shown in Fig. 1. The circumference of the ring is 30.9 m with dipole length of 1.6 m. The dipole is designed to be rectangular type, with sagitta for easy construction. Correctors and BPMs are installed in the gaps between dipoles and quadrupoles to leave more space in the longer drift for injection and extraction devices. The main parameters of the ring are summarized in Table 1. The optical function of one cell is shown in Fig. 2.

Besides its merits in free space and kick arm, this lattice shows other good properties. Its β function is well controlled, with the maximum value below 6 m in both planes, decreasing the requirement on magnet aperture. With a strong focusing structure, its transition energy $\gamma_T = 1.64$ is much higher than the maximum extraction energy $\gamma_{250 \text{ MeV}} = 1.27$.

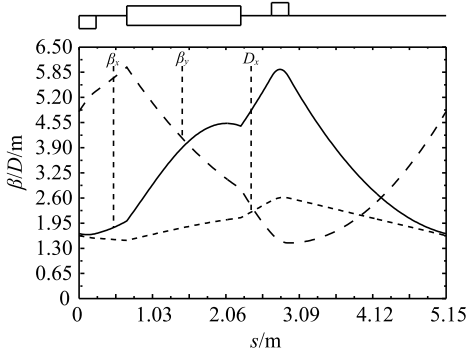


Fig. 2. The optical function of one DBFO cell. We choose FINT=0.5 in the design, while the focusing quadrupole can be used to compensate the realistic fringe field integral after the dipole is built.

Table 1. Parameters of the lattice.

parameter	value	unit
circumference	30.9	m
bending radius	1.519	m
dipole edge angle	30	°
injection energy, E_{inj}	7	MeV
extraction energy, E_{max}	250	MeV
$\hat{\beta}_x/\hat{\beta}_y/\hat{D}_x$ ¹	5.7/6.0/2.6	m
tune, ν_x/ν_y	1.68/1.78	
chromaticity, C_x/C_y	-0.2/-2.3	
transition energy, γ_T	1.64	

¹ $\hat{\beta}_x$ and $\hat{\beta}_y$ are the peak value of horizontal and vertical β function, respectively. \hat{D}_x is the peak value of the horizontal dispersion function.

3 Injection system

The maximum intensity a medium energy proton synchrotron can reach is limited by the strong space charge effect during the injection stage. A typical intensity requirement for proton therapy is 1×10^{11} protons per pulse (ppp). This target can be reached by multi-turn proton injection or multiturn strip injection. We prefer strip injection because it can reduce beam loss and provide better control over the beam emittance.

The space charge effect can be characterized by incoherent tune shift. Assuming the transverse distribution of the beam is Gaussian, incoherent tune shift is estimated by

$$\Delta\nu_{sc} = \frac{F_B N_B r_0}{4\pi\beta^2\gamma^3\epsilon} \quad (2)$$

where $F_B = C/\sqrt{2\pi}\sigma_s$ is the bunching factor, C is the circumference of the ring, σ_s is the root mean square bunch length, N_B is the number of particles per bunch, r_0 is the classical radius of proton, and ϵ is the emittance of the beam. As a typical criterion in low energy synchrotrons, the tune shift should not exceed 0.25. The systematic 4th order space charge resonance at 1.5 can be avoided by setting the ν_x at injection above 1.75. To reduce construction costs, the energy of the injector is usually 7 MeV. F_B is about 2 after longitudinal capture. To accumulate 2×10^{11} protons in one working period, beam emittance should be about 80π mm mrad to keep tune shift below 0.25.

3.1 Layout of injection system

Fig. 3 shows a schematic view of the injection system. The injection system is mainly composed of two types of bump magnet. One type is the chicane magnets (Ch1-3). Chicane magnets are used to produce a permanent horizontal offset at the injection point where carbon foil is installed. The other type is the pulsed dipole magnets

used for phase space painting. Two pulsed dipole magnets (Bumper1–2) installed on the ring with 180° phase advance can form a local horizontal bump. A pulsed dipole magnet (Bumper3) installed on the injection line 180° upstream of the injection point will produce an angle change in the vertical plane.

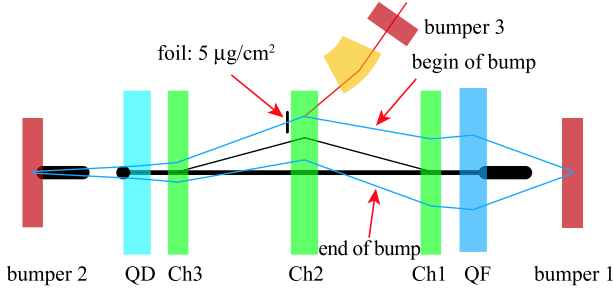


Fig. 3. (color online) Schematic view of injection system. The orbit varies from the positive side to the negative side during the painting process, to make full use of the focusing quadrupole aperture.

3.2 Painting scheme

The painting scheme is shown in Fig. 4. By gradually varying the orbit, the circulating beam is filled from the center to the boundary in horizontal phase space. The horizontal beam ellipse of the injection beam does not match the ring's, making the injection beam stay near the edge of acceptance of the circulating beam, and thus making the injection more uniform. Since the lattice design does not have reflection symmetry, the closed orbit will reach the maximum bump at the focusing quadrupole. To reduce the aperture of the focusing quadrupole at the injection section, the negative bump method is applied as shown in Figs. 3 and 4. The fields of the chicane magnets and bumpers do not ramp with the dipole and quadrupole, so the negative bump will gradually disappear with the ramping process. In the vertical plane, phase space is painted from outside to inside with the decay of vertical injection angle. The time function of the painting process is an exponential decay

$$x_{\text{paint}} = x_{\text{max}}(2e^{-\frac{t}{\tau}} - 1), \quad x'_{\text{paint}} = x'_{\text{max}}(2e^{-\frac{t}{\tau}} - 1) \quad (3)$$

$$y_{\text{paint}} = 0, \quad y'_{\text{paint}} = -y'_{\text{max}}e^{-\frac{t}{\tau}} \quad (4)$$

where $(x_{\text{max}}, x'_{\text{max}})$ and y'_{max} are the maximum phase space offset caused by the pulsed magnets, and τ is the decay time of the offset. The beam intensity of the linac is chosen to be about 5 mA, so 20 turns (about 16 μs) injection is sufficient to accumulate 2×10^{11} protons, with τ about 30 μs to match the design of transverse painting.

The painting process is simulated by ORBIT [10]. Fig. 5 presents the painting result. In the vertical plane, the painting process achieves good uniformity. In the horizontal plane, however, as the dispersion function

is not zero and a momentum spread ($\delta_{\text{rms}} = 0.15\%$) is included in the simulation, the final beam distribution looks like a Gaussian distribution with a long tail. Tune spread of the beam after injection is shown in Fig. 6. The initial distribution of the beam in the longitudinal direction is uniform, so the tune distribution is concentrated and the maximum shift is about 0.1 in both planes. After RF capture, with the bunching in the longitudinal direction, tune spread grows and reaches a maximum

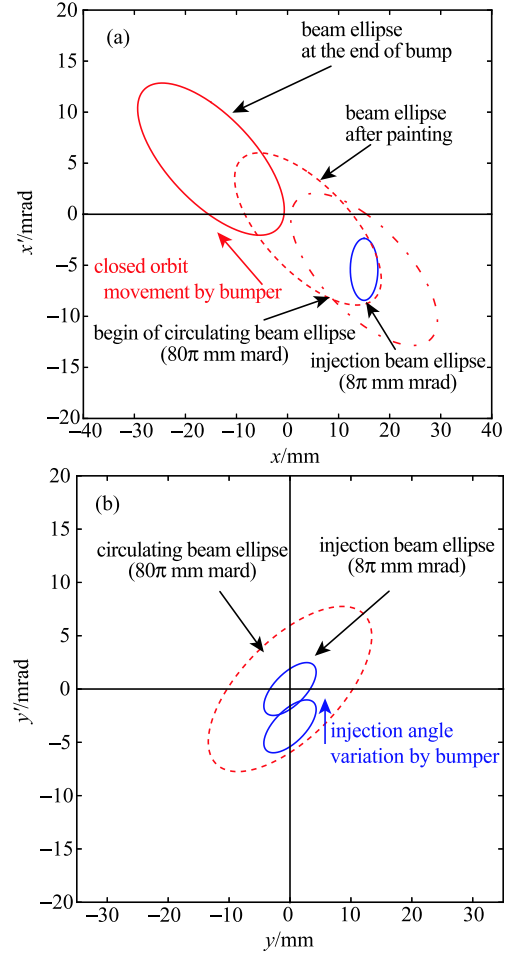


Fig. 4. (color online) Injection painting scheme in (a) horizontal phase space, (b) vertical phase space.

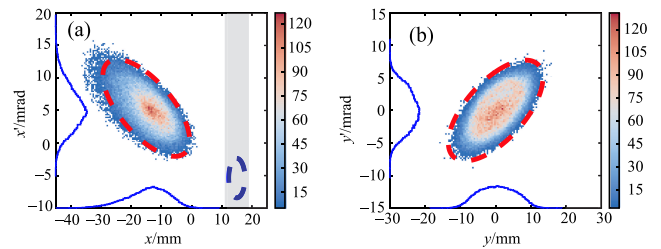


Fig. 5. (color online) Particle distribution after the painting process in (a) horizontal phase space and (b) vertical phase space.

shift of about 0.2 in both planes. The simulation result shows our painting scheme has achieved better uniformity than Gaussian distribution, keeping tune shift below 0.2. Thus we have set the horizontal work point around 1.70 during injection to avoid resonance at 1.50.

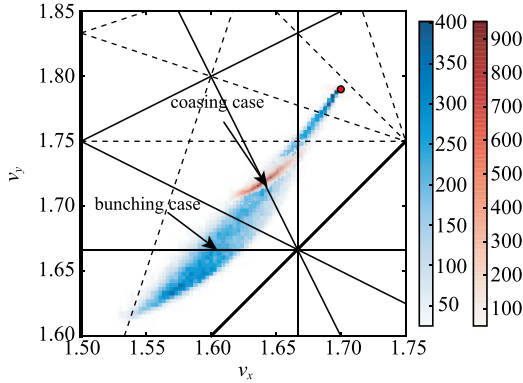


Fig. 6. (color online) Tune spread after injection. The horizontal work point has been tuned to 1.70 in the simulation.

4 Extraction system

We propose slow extraction using 3rd order resonance and RF-KO. The basic principle of this method is to apply a transverse RF field which resonates with the horizontal betatron tune of the particle, then the particle is kicked out of the separatrix produced by sextupoles. The transverse distribution of the extraction beam can keep constant by applying RF-KO and keeping the magnetic field constant. RF-KO can also provide good beam time structure with proper frequency modulation (FM) and amplitude modulation (AM)[11].

The parameters of the extraction system are listed in Table 2. The acceptance of the separatrix is set at 30π mm mrad to accommodate beam at the lowest extraction energy of 60 MeV. With a good kick arm of about 3 m, the design kick angle of the wire septum is 11 mrad, so the length and gap voltage of the wire septum is well below the critical value of the wire septum [12].

Table 2. Parameters of the extraction system.

parameter	value
separatrix	
extraction work point(x/y)	1.678/1.783
separatrix acceptance	30π mm mrad
spiral step	5 mm
septum	
kick angle of wire septum	11 mrad
gap width of wire septum	15 mm
length of wire septum	0.8 m
maximum gap voltage of wire septum	90 kV
thickness of magnetic septum	15 mm
RF-KO	
RF-KO FM method	dual FM
central tune of RF-KO, ν_{kick}	0.675
tune bandwidth of RF-KO, $\Delta\nu_{\text{kick}}$	0.015

4.1 Layout of extraction system

As discussed in Section 2, the location of the septums is fixed to optimize the kick arm. The remaining problem is making a triangular separatrix suitable for beam extraction. As shown in Fig. 1, a sextupole pair (SEA1/SEA2) is used for resonance driving and another sextupole pair (SEQ1/SEQ2) is used for chromaticity correction. Both pairs are arranged near the focusing quadrupoles to minimize their effects on the vertical plane. The position of the sextupole pair (SEA1/SEA2) is slightly away from the focusing quadrupole to adjust their phase advance to the wire septum. The normalized separatrix at the wire septum and magnetic septum are obtained by single particle tracking using MAD8, as shown in Fig. 7. The numbers in the figure label the edge of separatrix; “1” is the path along which the beam comes to the wire septum. By tuning the strength of sextupole pair (SEQ1/SEQ2), the orbits of particles with different momentum deviation at path “1” at the wire septum coincide, and thus the Hardt condition is satisfied.

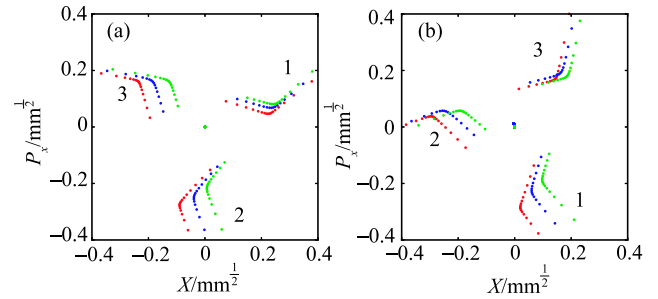


Fig. 7. (color online) Normalized separatrix at the septums: (a) at the wire septum and (b) at the magnetic septum. Red, blue and green dots correspond to particles with momentum deviation -0.001, 0.000, and 0.001 respectively.

4.2 Properties of extraction beam

FFT analysis of particle motion shows that, from the center to the separatrix boundary, betatron tune drops from 1.678 to 1.673. We applied the dual FM method to cover this tune region [14]. The dual FM method can be viewed as two single FMs with 180° phase difference. Each FM has a period of T_{FM} . The main component of ripple introduced by the dual FM method has a frequency of $2/T_{\text{FM}}$. To increase the ripple frequency, we propose a T_{FM} of 2500 turns. Corresponding to extraction energy of 60–250 MeV, $2/T_{\text{FM}}$ ranges from 2.66 kHz to 4.77 kHz, high enough for seconds-level radiation applications.

The properties of the extraction beam are further studied through multi-particle tracking. We have developed a tracking code in C++ language to conduct the

simulation. The tracking method we use is symplectic integration [16], which can preserve the nonlinear properties of the lattice and avoid numerical heating in long time simulations. The time structure of the extraction beam with different ν_{kick} and $\Delta\nu_{\text{kick}}$ was simulated. For each simulation set, 16000 particles were launched and extracted in 50000 turns. The strength of transverse RF was modulated during the extraction process to make the beam's time structure more uniform [13].

In Fig. 8, we present the extraction efficiency with different parameter settings. The system shows a narrow response bandwidth. Extraction is most efficient when ν_{kick} is 0.676 and $\Delta\nu_{\text{kick}}$ is 0.005. The parameter setting of best extraction efficiency is exactly consistent with the tune spread of the separatrix obtained from single particle tracking.

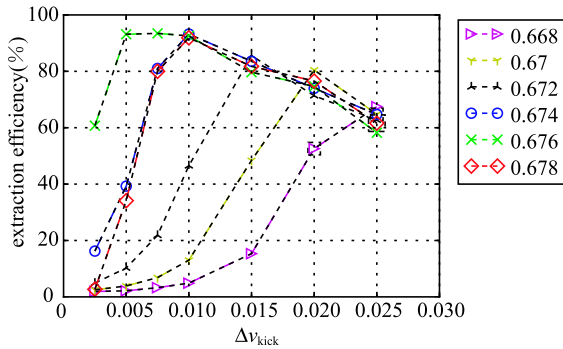


Fig. 8. (color online) Extraction efficiency with different ν_{kick} and $\Delta\nu_{\text{kick}}$

The uniformity of the extraction beam's time structure is strongly affected by $\Delta\nu_{\text{kick}}$, as shown in Fig. 9. The ripple caused by FM is significantly weaker when $\Delta\nu_{\text{kick}}$ is 0.015 than when it is 0.005 or 0.020. We investigate this phenomenon by studying snapshots of the phase space, as shown in Fig. 10. The particle distribution has a dense core surrounded by a sparse and uniform region when $\Delta\nu_{\text{kick}}$ is narrow. The distribution is chaotic when $\Delta\nu_{\text{kick}}$ is wider. It is inferred that the frequency component outside the particle's tune region has contributed to the motion, making distribution chaotic and suppressing the ripple of FM. When $\Delta\nu_{\text{kick}}$ gets too large, the effective kick occupies only a small part of the FM period. Although the particle distribution is chaotic, the extraction can happen only when the kick is effective, so the FM ripple will re-dominate the time structure.

The extraction beam ripple is evaluated by

$$R = \frac{\sigma_{\text{bin}}}{\mu_{\text{bin}}} \quad (5)$$

where μ_{bin} is the average number of events in the histogram bins, and σ_{bin} is the standard deviation of the number of events. The ripple level of each simulation set measured by R is presented in Fig. 11. The bin width

is 100 turns, small enough to evaluate the ripple caused by FM. With sufficient simulation particles, each bin has accumulated enough events to reduce statistical fluctuation. R is calculated with bin index from 200 to 300 (corresponding to turns 15000 to 25000) to exclude the effects of global beam ripple. The statistical result shows that, for ripple level consideration, ν_{kick} around 0.675 is better than other options. The ripple level drops significantly when $\Delta\nu_{\text{kick}}$ grows from 0.005 to 0.010, and reaches a minimum value when $\Delta\nu_{\text{kick}}$ is around 0.010–0.015.

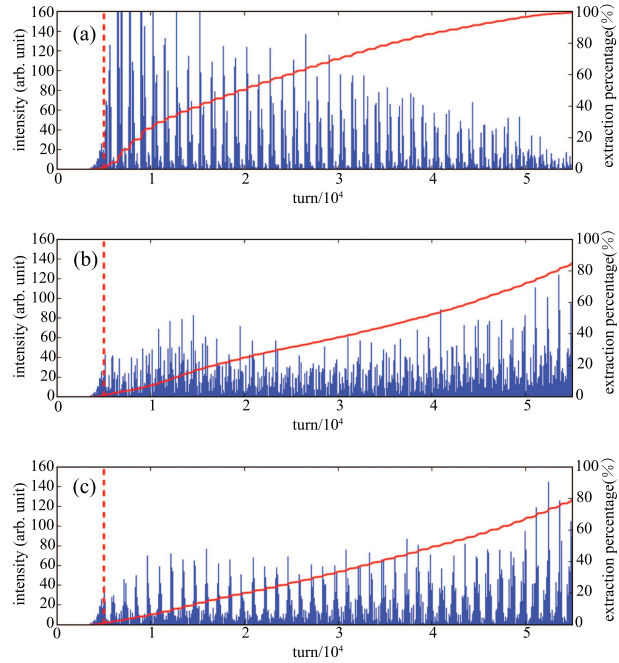


Fig. 9. (color online) Time profile of extraction beam with different $\Delta\nu_{\text{kick}}$. ν_{kick} is 0.676 for each case, and $\Delta\nu_{\text{kick}}$ is (a) 0.005, (b) 0.015 and (c) 0.020. The width of each bin is 100 turns. The red lines plot the extraction percentage with increasing number of extraction turns. The first 5000 turns are used for sextupole ramping, so few particles are extracted.

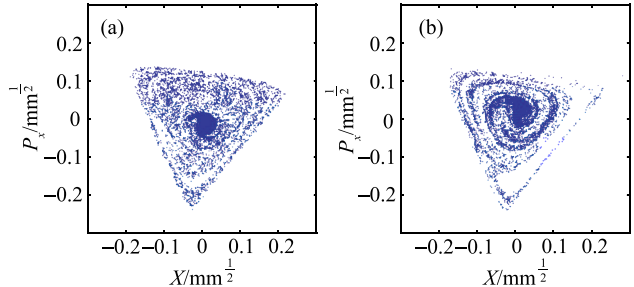


Fig. 10. (color online) Phase snapshots with different $\Delta\nu_{\text{kick}}$. ν_{kick} is 0.676 for each case, and $\Delta\nu_{\text{kick}}$ is (a) 0.005 and (b) 0.015. The snapshots were taken when extraction efficiency was about 60%.

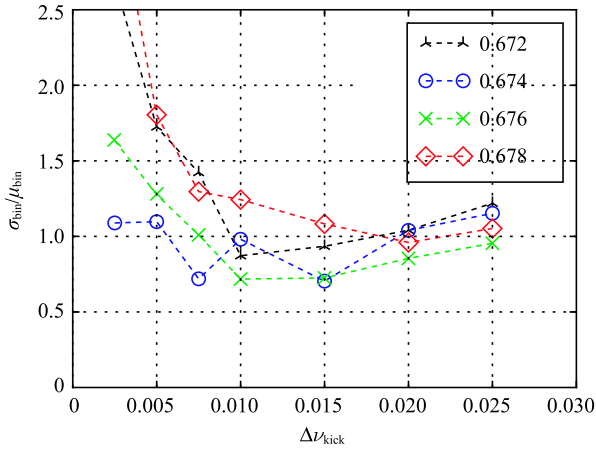


Fig. 11. (color online) Beam ripple level with different ν_{kick} and $\Delta\nu_{\text{kick}}$

In conclusion, we choose ν_{kick} to be 0.675 and $\Delta\nu_{\text{kick}}$ to be 0.015. While losing some power efficiency, wide $\Delta\nu_{\text{kick}}$ has improved the quality of the extraction beam. For long time extraction, the kick angle each turn is around the μrad level, so the power wastage should not cause serious problems. Methods like the separate function method [14] can be applied to further improve the quality of the extraction beam.

5 Summary

We have presented the design and simulation results of a compact proton synchrotron.

The lattice structure has provided much continuous free space and achieved a decent kick arm. It also shows good properties like small β function, large transition energy and easy tuning. We believe this lattice structure would be a good option for other projects with similar applications.

We have designed the layout of a strip injection system and a scheme for phase space painting. The simulation results show that this scheme can control the tune spread below 0.2 with an intensity of 2×10^{11} ppp.

A slow extraction system using 3rd order resonance and RF-KO was discussed. The parameters of the RF-KO system were optimized through particle tracking to achieve both good extraction efficiency and time microstructure.

The authors would like to thank Prof. Shouxian Fang, Prof. Jingyu Tang of IHEP, Dr. Manzhou Zhang of SINAP and Prof. Shyh-Yuan Lee of Indiana University for their advice on lattice design and slow extraction.

References

- G. R. Li, X.L. Guan et al. *Morden Applied Physics*, **6**(2): 85–89 (2015)
- F. Cole, P. V. Livdahl et al, Design and Application of a Proton Therapy Accelerator. in *Proceedings of PAC 1987*, p. 1985–1987
- L. Badano, M. Benedikt et al. Proton-ion Medical Machine Study(PIMMS), Part I. Cern report CERN/PS, 99–010 (1999)
- K. Endo, Z. Fang et al. Compact Proton and Carbon Ion Synchrotrons for Radiation Therapy, in *Proceedings of EPAC 2002*, p. 2733
- Nader Al Harbi and S. Y. Lee, *Rev. Sci. Instrum*, **74**(4): 2540–2545 (2003)
- K. Hiramoto, M. Umezawa et al, *Nucl. Instrum Methods in Phys. Res. B*, **261**: 786–790 (2007)
- S. X. Fang, X. L. Guan et al, *CPC(HEP & NP)*, **34**: 383–388 (2010)
- S. Y. Lee, *Accelerator Physics*, (Third edition, Singapore: World Scientific Publishing Company, 2011)
- S. Y. Lee, W.M. Tam, and Z. Liu. *Rev. Sci. Instrum*, **78**: 096104 (2007)
- J. Galambos, S. Danilov et al. ORBIT – A Ring Injection Code with Space Charge, in *Proceedings of PAC99*, p. 3143-3145
- K. Noda, M. Kanazawa et al, *Nucl. Instrum Methods in Phys. Res. A*, **374**: 269–277 (1996)
- M. J. Barnes, J. Borburgh et al, Injection and Extraction Magnets: septa, arxiv: 1103, 1062
- T. Furukawa, K. Noda et al. *Nucl. Instrum Methods in Phys. Res. A*, **522**: 196–204 (2004)
- K. Noda, T. Furukawa et al, *Phys. Res. A*, **492**: 241–252 (2002)
- K. Noda, T. Furukawa et al, *Phys. Res. A*, **492**: 253–263 (2002)
- E. Forest. *J. Phys. A: Math. Gen.*, **39**: 5321–5377 (2006)